Active optics null test system based on a liquid crystal programmable spatial light modulator

Miguel Ares,* Santiago Royo, Irina Sergievskaya, and Jordi Riu

Centre for Sensors, Instrumentation and Systems Development (CD6), Universitat Politècnica de Catalunya (UPC—Barcelona Tech), Rambla Sant Nebridi 10, 08222 Terrassa, Spain

*Corresponding author: miguel.ares@oo.upc.edu

Received 2 August 2010; revised 28 September 2010; accepted 30 September 2010; posted 5 October 2010 (Doc. ID 132789); published 2 November 2010

We present an active null test system adapted to test lenses and wavefronts with complex shapes and strong local deformations. This system provides greater flexibility than conventional static null tests that match only a precisely positioned, individual wavefront. The system is based on a cylindrical Shack–Hartmann wavefront sensor, a commercial liquid crystal programmable phase modulator (PPM), which acts as the active null corrector, enabling the compensation of large strokes with high fidelity in a single iteration, and a spatial filter to remove unmodulated light when steep phase changes are compensated. We have evaluated the PPM's phase response at 635 nm and checked its performance by measuring its capability to generate different amounts of defocus aberration, finding root mean squared errors below $\lambda/18$ for spherical wavefronts with peak-to-valley heights of up to 78.7λ, which stands as the limit from which diffractive artifacts created by the PPM have been found to be critical under no spatial filtering. Results of a null test for a complex lens (an ophthalmic customized progressive addition lens) are presented and discussed.

OCIS codes: 110.1080, 120.0120, 120.3940, 120.4630.

1. Introduction

A growing number of complex-shaped lenses that are being introduced on the market outperform classical optical systems with spherical surfaces. They range from technical optics examples in the form of complex optical designs with folded aspheric surfaces for compact imaging [1] to free-form optical surfaces that maximize the performance of the conventional progressive addition lenses on the ophthalmic market, customizing the lens to a variety of parameters depending on the patient and the use to which the lens is put [2]. As the production of complex-shaped lenses has increased in recent years, so has the demand for an appropriate measurement of shape as part of the quality control process, as lenses cannot be manufactured better than they are measured. To date, a common way to optically test high-quality aspheric lenses and mirrors is still to use null correctors within a high-resolution measurement system (typically an interferometer), in order to compensate the aspheric wavefront being tested, and, subsequently, to use an interferometer to control the theoretically flat wavefront. The deviations from the resulting null interferogram reflect the problems encountered in the manufacturing process, given the null corrector is both perfect and properly positioned. Therefore, the accuracy of the resulting null test is strongly dependent on the accuracy of the prepared null corrector, an effect that is well known in classical optical shop work [3]. Although a number of configurations for conventional null correctors are available, they normally consist of one or more precisely manufactured lenses or mirrors that, once positioned, implement the required compensation. Alternative null correctors have been proposed in the form of diffractive elements created with computer-generated holograms [4]. In these elements, the ideal aspheric shape is computationally generated as a wrapped phase map and then written on a substrate using lithographic equipment, such as a direct laser

0003-6935/10/326201-06$15.00/0

writing system or an electron-beam writer. However, neither refractive nor diffractive static null correctors are an economic solution for the industry in terms of money or time, in that an individual null corrector must be produced for each aspheric or free-form design. In addition, the advent of numerically controlled machines has spread the fabrication of free-form surfaces of practically any required shape that are custom made to the application, making large production series increasingly rare.

To overcome this limitation, alternatives to static null correctors based on dynamic phase modulator devices, such as deformable mirrors or liquid crystal spatial light modulators, have been proposed for a rapid and flexible characterization of complex-shaped optics [5,6]. Among these types of devices, parallel-aligned liquid crystal phase-only modulators (LCMs) have become an established commercial technology with promising specifications for active null correction. Parallel-aligned LCMs operate by spatially changing the refractive index of the liquid crystal and, as a consequence, modifying the phase of the incoming wavefront. Commercial parallel-aligned LCMs offer significant advantages over both twisted-nematic liquid crystal displays (e.g., more efficient phase modulation) and deformable mirrors (e.g., superior spatial resolution, a larger effective stroke through the use of 2π wrapped phase maps, or higher phase fidelity, which enables the direct generation of the required wavefront shape with no need for feedback) [7,8]. Among the drawbacks, unwanted diffractive orders of light become more significant as the local phase changes generated become steeper [9,10]. In this paper, we describe an active null test system based on the combination of a modified Shack–Hartmann wavefront sensor, a programmable phase modulator (PPM) as a null corrector, and a spatial filter to remove spurious diffractive effects.

The paper is organized as follows. Section 2 describes the active null test setup. Section 3 shows the experimental results for the phase response characterization of the PPM. Section 4 presents the system's performance as a null corrector through the full compensation of the wavefront created by a customized progressive addition lens, which is used as an example of a complex lens. Finally, Section 5 summarizes the main conclusions of the work.

2. Active Null Test System

The introduction of a null corrector within an optical metrology system for testing lenses is intended to provide a null result of measurement, making deviations from the expected shape easily detectable. Normally, this is done through the manufacture of an optical device that, when combined with the wavefront under test, turns it into a flat wavefront so that deviations from the ideal shape can be easily detected by classical optical shop tests [11]. The null test setup we propose consists of the use of a cylindrical Shack–Hartmann wavefront sensor (CSHWS) as the optical shop test, together with a liquid crystal PPM acting as the active null corrector. The CSHWS provides a large dynamic range of measurement based on the continuity of the focal lines detected, to cope with highly aberrated wavefronts from lenses with complex shapes or with strong local deformations. The principle of the CSHWS developed is described in detail in the literature [12]. The PPM device performs the active null correction by generating the negative of the phase to be compensated in a computer image, in the form of an 8 bit gray-level wrapped phase map. This image is sent from the computer to the device via a video graphics array connection.

The experimental configuration of the complete null test arrangement is shown in Fig. 1. A 635 nm point light source obtained from a pigtailed laser diode is collimated using an achromatic doublet (L1). The resulting flat wavefront passes through a linear polarizer (P), crosses the complex lens to be tested (O), and is directed toward the PPM by means of a pellicle beam splitter (BS1) that does not alter the optical path length. Afterward, the deformed wavefront is compensated by the PPM, which is conjugated with the CSHWS through a telescope system made up of two doublets with focal lengths of 200 and 50 mm (L2 and L3, respectively). The CSHWS is composed of two equivalent arrays of microcylinders (focal length $= 7.9$ mm, pitch $= 0.3$ mm) oriented along the horizontal (X) and vertical (Y) directions so that they are arranged orthogonally. The CSHWS samples the incoming plane wavefront once it has been divided by a second pellicle beam splitter (BS2), yielding two patterns of straight focal lines, one oriented along X and the other along Y. These focal line patterns are simultaneously recorded by two equivalent monochrome CCD cameras placed behind each of the two arrays of microcylinders. Insofar as a flat wavefront is expected, a pattern of equidistant horizontal and vertical lines should be present at the CCD cameras. The patterns are then processed using an algorithm that follows the next steps. First, a segmentation procedure separates the lines from the background.

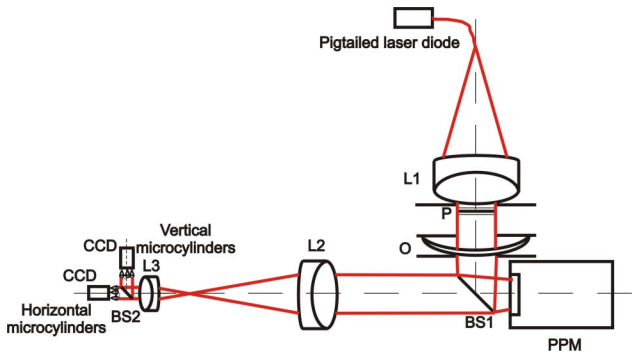

Fig. 1. (Color online) Scheme of the active null test system for testing complex-shaped lenses. The linearly polarized wavefront transmitted by lens O is fully compensated with a liquid crystal PPM, whose molecules are parallel to the beam polarization. A telescope formed by lenses L2 and L3 conjugates the PPM with a cylindrical Shack–Hartmann sensor, which measures the wavefront.

Second, the lines are identified due to their continuity by labeling them with consecutive numbers starting from the central line. Third, by means of a center-of-mass computation, the centroids in the X and Y directions are computed for the vertical and horizontal line images, respectively, but in the domain given by the intersection between both line images. Afterward, as far as the Shack–Hartmann sensor needs a reference wavefront to be able to compute the resultant null test wavefront, the last three steps are also done for a plane reference wavefront created within the system with the PPM acting as a mirror and the lens O removed from the active null test setup of Fig. 1. The relative displacement between the null test's and reference's X and Y centroids are then computed for calculating the wavefront slopes in the X and Y directions, respectively. Thus, this relative measurement using an experimental reference wavefront ensures the correct matching of the results taken in both arms of the CSHWS. Finally, the final wavefront is reconstructed from the wavefront slopes in terms of circular Zernike polynomials up to the fifth order using a singular value decomposition technique [13].

3. PPM Phase Response

A. Phase Modulation Characteristics of the PPM

The dynamic null corrector in the setup shown in Fig. 1 is the PPM, an optically addressed phase modulator based on a parallel-aligned liquid crystal (LC), whose structure and operation has been described elsewhere [9]. In order to achieve a phase-only modulation, the incident wavefront needs to be linearly polarized in the direction of the liquid crystal's parallel molecules when no electric field is applied. This is the PPM's normal working mode and the one used in the null test setup presented in Fig. 1. However, to characterize the PPM's phase response, an amplitude modulation working mode is used. The PPM is illuminated by a linearly polarized beam with the axis oriented at 45° from the axis of the molecules in the liquid crystal layer in the unbiased state (meaning that polarizer P in Fig. 1 is rotated 45°), and an analyzer (A), oriented orthogonally to polarizer P, is inserted just after the PPM. In this configuration, changes in the light intensity transmitted by the analyzer may be directly related to the cosine of the phase changes induced on the PPM [9]. Induced phase changes are controlled by the gray level written onto the PPM, ranging from a full-screen null phase change when black (0) to a maximum phase change when white (255). Considering a linear relationship between the phase change φ and the gray level G, one can evaluate the linear coefficient α that relates the two parameters by fitting a sinusoidal function to the transmitted intensity I for a series of uniform gray-scale images displayed in the PPM, according to

$$I = \frac{I_{\max} + I_{\min}}{2} - \frac{I_{\max} - I_{\min}}{2}\cos(\alpha G + \alpha 2\varphi_0), \quad (1)$$

where $I_{\min}$ and $I_{\max}$ are the minimum and maximum transmitted intensities, and φ_0 is the PPM's phase in the unbiased state. The intensity transmitted by the analyzer is measured with a lensless CCD camera that images the PPM surface through doublet L2. With the aid of a Z axis linear positioning stage, the CCD is accurately positioned close to the image focus of doublet L2 in a position that fits the size of the CCD to the size of the light beam coming from the PPM. Although some of the components of this calibration setup, depicted in Fig. 2, are different from those of the null test system shown in Fig. 1, most of the components present in both setups remain untouched. This ensures that the PPM phase response is evaluated under the same conditions under which it will perform the null correction in the experiment.

To characterize the PPM's phase modulation, a set of 27 uniform gray-scale maps, ranging from 0 to 255, were written on it, and the transmitted intensity was averaged over the pixels of the camera sensor. Consequently, potential nonuniformities in the diode laser beam, polarizers, doublets, camera sensor, and liquid crystal surface were averaged, and a global value for the coefficient relating the phase change and the gray level was obtained, which is a common procedure in these types of systems [7,10,14]. Figure 3 shows the sinusoidal fit of the recorded intensity as a function of the gray level displayed in the PPM. A linear coefficient $\alpha = 0.0266 \pm 0.0003$ is obtained, allowing a phase modulation range of $2.16\pi \pm 0.02\pi$ rad at $\lambda = 635$ nm, equivalent to a path length variation of 1.08 ± 0.01 wavelengths. The regression coefficient obtained (0.990) confirms the validity of the model in Eq. (1).

B. PPM Performance for Aberration Generation

Once the PPM's phase modulation response has been calibrated, it is important to evaluate its capability to

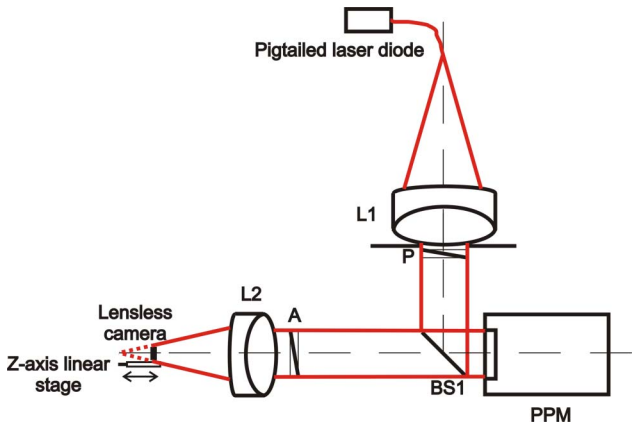

Fig. 2. (Color online) Scheme characterizing the phase response of the PPM in an intensity modulation working mode. A lensless camera positioned close to the image focus of doublet L2 collects the light transmitted by an analyzer (A) for the different uniform gray-level maps displayed in the PPM. The analyzer was oriented orthogonally to linear polarizer P, which was placed at 45° relative to the orientation of the molecules of the PPM.

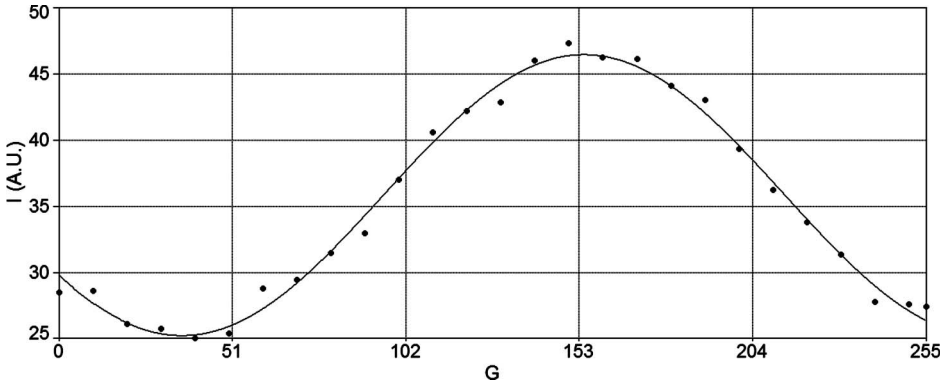

Fig. 3. Sinusoidal fitting of the mean intensity (I) recorded by the camera sensor as a function of the uniform gray-level maps (G) displayed in the PPM.

generate real aberrations within the active null test setup developed when wrapped phase maps are used. With lens O removed from the active null test setup of Fig. 1, ideal spherical phase maps with peak-to-valley heights of 19.7λ, 39.4λ, and 78.7λ were displayed into the PPM and measured using the CSHWS. The quality of the aberrations generated by the PPM was evaluated as the root mean squared (RMS) error between the ideal spherical phase map written in the PPM and the real spherical wavefront measured by the CSHWS. Results for ideal and real wavefronts are presented in Table 1. For the different amplitudes of defocus aberration analyzed, RMS errors stayed below $\lambda/18$, showing the PPM's capability to generate wavefronts in an open loop configuration with no need for additional iterations. In fact, the results are indicative of the PPM's wavefront generation performance within the null setup developed, which includes the CSHWS, in that the spherical wavefront is measured relative to a plane reference wavefront previously detected when a flat gray-scale map was written in the PPM. Thus, potential deviations from the flatness of the PPM surface might be practically canceled in the Shack–Hartmann method, insofar as these errors are present both in the aberrated and reference wavefronts [15,16].

The PPM's ability to reproduce the wavefront in a wrapped phase map representation enables large phase changes to be generated. However, in practice, this is limited by the appearance of diffraction artifacts that become more significant as the amplitude of the aberration to be generated increases. Reproducing steep phase changes with a small number of pixels considerably reduces the device's diffraction efficiency, so that the light modulated by the PPM becomes less intense than the unmodulated original wavefront. This creates a double image that combines the modulated (desired) and unmodulated (undesired) diffracted wavefronts in different amounts. This behavior has been observed to be critical for spherical wavefronts with peak-to-valley heights from 78.7λ, where the line patterns associated with the unmodulated original wavefront are significantly superimposed on those of the modulated spherical beam of interest and, as a consequence, the automatic line-tracking algorithm fails to process the image data. To overcome this problem, which occurs when large aberrations are compensated, a pinhole acting as a spatial filter was introduced in the null test setup, as described in the next section.

Table 1. PPM Performance for the Generation of Different Defocus Aberrations within the Null Test System Developed

Peak-to-Valley Amplitude (Waves)	RMS Error (Waves)
19.7	0.02
39.4	0.03
78.7	0.05

4. Null Correction of a Customized Progressive Addition Lens

To show the capabilities of the null test system, the total compensation of the wavefront transmitted by a commercial ophthalmic progressive addition lens (PAL) is presented as an example of a complex lens on the market. The right eye (RE) PAL (Varilux Ipseo, Essilor International, France) with nominal null far vision power and +2.00 D power addition (Add), had a design customized for presbyopic wearers who mainly move their head rather than their eyes when performing visual tasks. To evaluate the wavefront to be nulled, we first measured the wavefront transmitted by the PAL using the CSHWS with the PPM acting as a mirror. In a second step, we made the null correction by displaying the corresponding conjugated phase map on the PPM. Because of the system's configuration, the null test was carried out for a central circular area of the lens with a diameter of 20 mm containing the 16 mm long power progression corridor and part of the temporal and nasal sides. Figures 4(a) and 4(b) show the line patterns detected by the CSHWS and the reconstruction of the original wavefront transmitted by the PAL, respectively. As expected, in the near vision region, where the addition reaches +2.00 D, the width of the lines increases from the diffraction-limited size, and they are also considerably deviated from a straight shape. The wavefront shape for this lens has a total height change of over 100λ peak to valley. Using the phase modulation constant obtained with

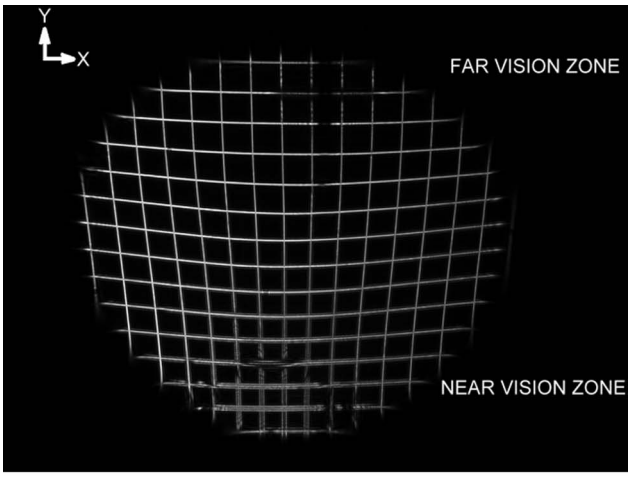

(a)

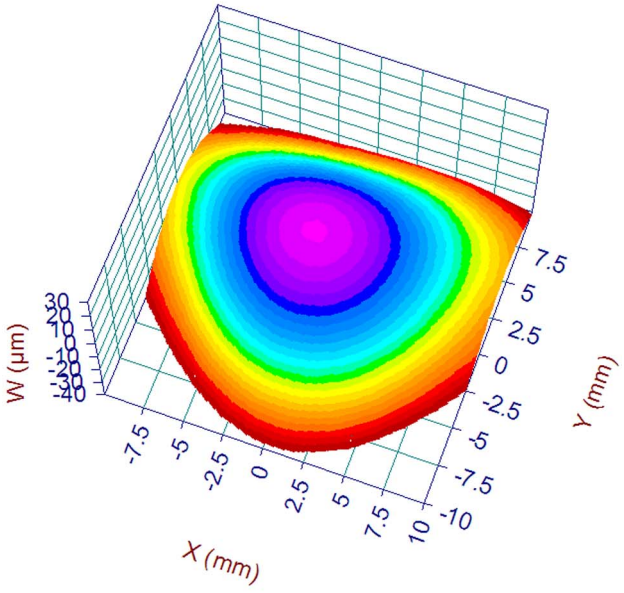

(b)

Fig. 4. (Color online) (a) Line patterns associated with the wavefront transmitted by a Varilux Ipseo PAL custom designed for headmover users. The line patterns were detected by the cylindrical Shack–Hartmann wavefront sensor with the PPM acting as a mirror. (b) Reconstruction of the wavefront.

the procedure described in Subsection 3.A, the conjugated wavefront was calculated in a wrapped grayscale representation and displayed in the PPM in order to carry out the null correction. Because of the large aberrations involved, diffraction artifacts became noticeable, and the unmodulated original wavefront became superimposed on the desired plane wavefront obtained as a result of the null correction. Figure 5(a) shows the original complex line pattern image detected by the CSHWS. In this case, the line-processing algorithm was unable to properly identify the lines associated with the resulting plane wavefront. To solve this problem, a circular pinhole filter was introduced in the setup, centered with the optical axis of the PPM-CSHWS path and positioned

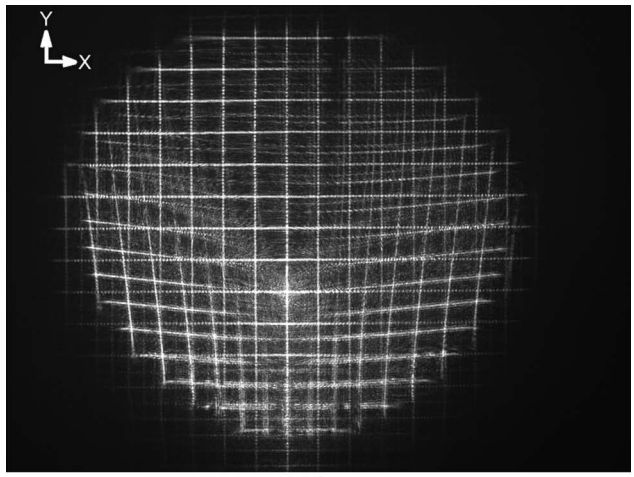

(a)

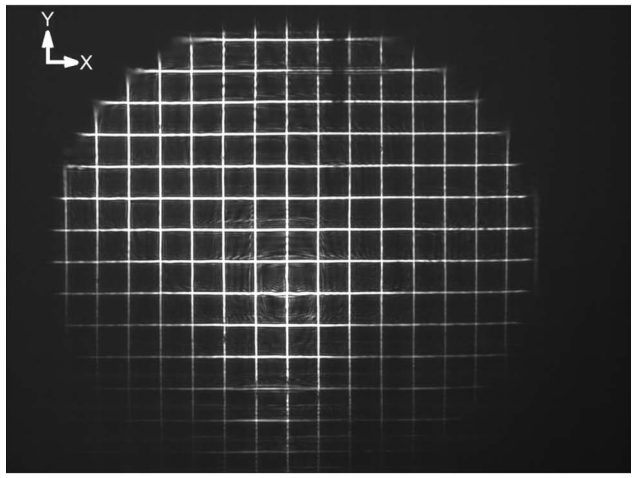

(b)

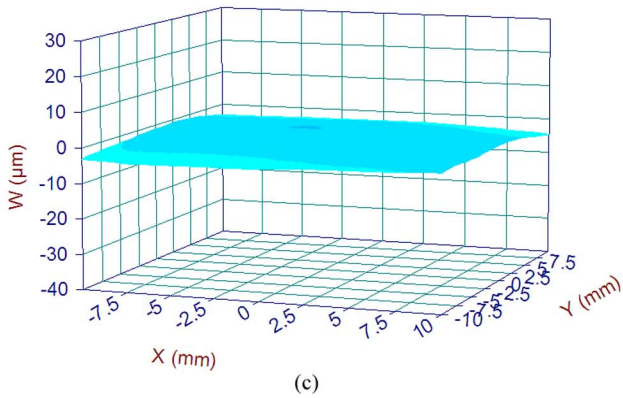

(c)

Fig. 5. (Color online) Line pattern associated with the light that the PPM outputs when the conjugated phase map of the PAL is displayed on it (a) without and (b) with the pinhole filter introduced in the setup. (c) Reconstruction of the resulting null wavefront, which has an RMS error from an ideal flat surface of $\lambda/12$.

in the image focal plane of doublet L2 of the telescopic system. When the circular pinhole filter is introduced in the setup, the unmodulated wavefront is blocked and only the on-axis light corresponding to the resulting plane wavefront reaches the CSHWS. Standard pinholes with diameters of 50, 100, 300, 500, and 1000 μm were experimentally tested. The

300 μm pinhole proved best for transmitting the lower spatial frequencies (central light spot) corresponding to the nulled wavefront while cropping the higher frequencies (light surrounding the central spot) associated to the PAL-shaped unmodulated wavefront. The straight-line image detected by the sensor when the 300 μm pinhole was inserted in the null test setup is shown in Fig. 5(b), showing a clear pattern that can be processed with the line processing algorithm. The final reconstruction of the corresponding wavefront is depicted in Fig. 5(c). The RMS error from a perfect flat surface is $\lambda/12$, which corresponds to 0.08% of the peak-to-valley height of the original wavefront.

5. Conclusions

We have presented an active optics null test system particularly suited for testing complex-shaped lenses yielding locally deformed wavefronts. The developed benchtop prototype consists of a CSHWS as a measurement system, a commercial liquid crystal PPM as the active null corrector, and a pinhole spatial filter. The programmable diffractive corrector provides a large effective stroke by representing the correction as a 2π wrapped phase map and has very good capabilities for reproducing wavefronts in open loop. However, steep strokes are badly reproduced due to the small number of pixels used to approximate them, reducing the device's diffraction efficiency. As a consequence, the unmodulated and modulated light diffracted by the PPM become mixed, making it very difficult to process the data. The problem is solved by including a pinhole spatial filter in the setup. We evaluated the quality of the PPM for wavefront manipulation by generating ideal spherical phase maps. For a set of spherical phase maps with peak-to-valley heights of 19.7λ, 39.4λ, and 78.7λ, RMS errors below $\lambda/18$ were obtained. Finally, the null test of an ophthalmic customized PAL with prescription RE + 0.00 Add + 2.00 was performed. The total compensation of such a wavefront with changes of over 100λ peak to valley was obtained with the presented setup. Because of the larger aberrations involved, a pinhole with a diameter of 300 μm was inserted to filter the unmodulated light diffracted by the PPM. This pinhole size showed experimentally the best performance in the setup to transmit the central light spot from the null wavefront while blocking the surrounding light corresponding to the unmodulated PAL wavefront. The reconstructed flat wavefront yielded an RMS error of $\lambda/12$ when compared to an ideal flat surface, showing the system's capacity to be used as an active null test.

The authors thank the Spanish Ministry of Science and Innovation for project DPI2009-13379, which funded this research. Miguel Ares acknowledges the Spanish Ministry of Education for grant AP2003-3140, which also supported this research.

References

1. E. J. Tremblay, R. A. Stack, R. L. Morrison, and J. E. Ford, "Ultrathin cameras using annular folded optics," Appl. Opt. **46**, 463–471 (2007).
2. D. Meister and R. Fisher, "Progress in the spectacle correction of presbyopia. Part 2: modern progressive lens technologies," Clin. Exp. Optom. **91**, 251–264 (2008).
3. D. Malacara, K. Creath, J. Schmit, and J. C. Wyant, "Testing of aspheric wavefronts and surfaces," in *Optical Shop Testing,* 3rd ed., D. Malacara, ed. (Wiley, 2007).
4. H. J. Tiziani, S. Reichelt, C. Pruss, M. Rocktaschel, and U. Hofbauer, "Testing of aspheric surfaces," Proc. SPIE **4440**, 109–119 (2001).
5. H. J. Tiziani, T. Haist, J. Liesener, M. Reicherter, and L. Seifert, "Application of SLMs for optical metrology," Proc. SPIE **4457**, 72–81 (2001).
6. C. Pruss and H. J. Tiziani, "Dynamic null lens for aspheric testing using a membrane mirror," Opt. Commun. **233**, 15–19 (2004).
7. P. M. Prieto, E. J. Fernández, S. Manzanera, and P. Artal, "Adaptive optics with a programmable phase modulator: applications in the human eye," Opt. Express **12**, 4059–4071 (2004).
8. M. T. Gruneisen, M. B. Garvin, R. C. Dymale, and J. R. Rotge, "Mosaic imaging with spatial light modulator technology," Appl. Opt. **45**, 7211–7223 (2006).
9. F. H. Li, N. Mukohzaka, N. Yoshida, Y. Igasaki, H. Toyoda, T. Inoue, Y. Kobayashi, and T. Hara, "Phase modulation characteristics analysis of optically-addressed parallel-aligned nematic liquid crystal phase-only spatial light modulator combined with a liquid crystal display," Opt. Rev. **5**, 174–178 (1998).
10. E. J. Fernández, P. M. Prieto, and P. Artal, "Wave-aberration control with a liquid crystal on silicon (LCOS) spatial phase modulator," Opt. Express **17**, 11013–11025 (2009).
11. D. Malacara and A. Cornejo, "Null Ronchi test for aspherical surfaces," Appl. Opt. **13**, 1778–1780 (1974).
12. M. Ares, S. Royo, and J. Caum, "Shack–Hartmann sensor based on a cylindrical microlens array," Opt. Lett. **32**, 769–771 (2007).
13. W. H. Press, S. A. Teukolsky, W. T. Vetterling, and B. P. Flannery, *Numerical Recipes: the Art of Scientific Computing,* 3rd ed. (Cambridge U. Press, 2007).
14. M. T. Gruneisen, L. F. DeSandre, J. R. Rotge, R. C. Dymale, and D. L. Lubin, "Programmable diffractive optics for wide-dynamic-range wavefront control using liquid-crystal spatial light modulators," Opt. Eng. **43**, 1387–1393 (2004).
15. D. R. Neal, D. J. Armstrong, and W. T. Turner, "Wavefront sensors for control and process monitoring in optics manufacture," Proc. SPIE **2993**, 211–220 (1997).
16. G. Y. Yoon, T. Jitsuno, M. Nakatsuka, and S. Nakai, "Shack–Hartmann wave-front measurement with a large F-number plastic microlens array," Appl. Opt. **35**, 188–192 (1996).